Forced convection in banks of inclined cylinders at low Reynolds numbers

A. J. Fowler and A. Bejan
Department of Mechanical Engineering and Materials Science, Duke University, Durham, NC, USA

This study documents the pressure drop and heat transfer through bundles of parallel cylinders in a domain that has been overlooked, namely, low Reynolds numbers, arrays that are long in the direction of flow such that the flow is hydraulically and thermally fully developed, and cylinders inclined relative to the flow direction. The numerical results cover the range $1 \leq Re_D \leq 30$, $0.72 \leq Pr \leq 100$, $0.6 \leq \phi \leq 0.95$ and $0° \leq \beta \leq 60°$, where ϕ is the porosity of the bundle as a saturated porous medium, and β is the angle between the cylinder centerline and the direction perpendicular to the flow direction. The accuracy is verified by means of experimental measurements of the pressure drop across a bundle with 115 cylinders in the flow direction, in the range $8 < Re_D < 50$, $0.84 \leq \phi \leq 0.92$ and $0° \leq \beta \leq 60°$. The results show that significant errors may occur if the available large-Re_D information is extrapolated to the domain covered by this study.

Keywords: yawed cylinder arrays; cross-flow; low Reynolds number

Introduction

This article documents the flow and heat-transfer characteristics of bundles of parallel cylinders that are inclined relative to the free stream that bathes them. The emphasis is on (1) the low Reynolds number range $Re_D \leq 30$, (2) the fully developed regime, and (3) the effect of the angle of inclination on the pressure drop and heat-transfer coefficient. These aspects have been overlooked despite the large research effort that has been devoted to banks of cylinders in cross-flow. The progress on this general topic has been reviewed by Zukauskas (1972, 1987a, b) and Kays and London (1984).

In his more recent review, Zukauskas (1987b) proposed a correction factor to account for the effect of angle of inclination on pressure drop calculations. It is unclear whether his method is universally valid, or applies only to a certain range of Reynolds numbers and a certain type of cylinder array. One objective of the present study was to clarify the conditions under which Zukauskas's correction is applicable.

The flow and heat-transfer results assembled in this article were developed in three phases. First, numerous cases of the flow and temperature fields in long bundles of inclined cylinders were simulated numerically, based on detailed three-dimensional (3-D) calculations. In the second phase, the heat and fluid-flow results were correlated into a saturated porous medium model that accounts for the angle of inclination and the low Reynolds number range. The third phase was experimental, where the accuracy of the numerical results was tested against laboratory measurements of the pressure drops through bundles at several cylinder inclinations and Reynolds numbers.

Address reprint requests to Professor Bejan at the Department of Mechanical Engineering and Materials Science, Duke University, Box 90300, Durham, NC 27708-0300, USA.

Received 8 October 1993; accepted 8 December 1993

Mathematical formulation

The numerical part of the study refers to an array of staggered cylinders, with their centers arranged in an array of equilateral triangles. Two orientations of the flow relative to the array were examined (Figure 1, *top*). The entire array was tilted to an angle β that varied from 0° to 60° relative to the perpendicular (Figure 1, *bottom*). In the numerical simulations (and unlike in the experiments; see later discussion) the spacing between cylinders was fixed so that the porosity of the bundle ϕ was

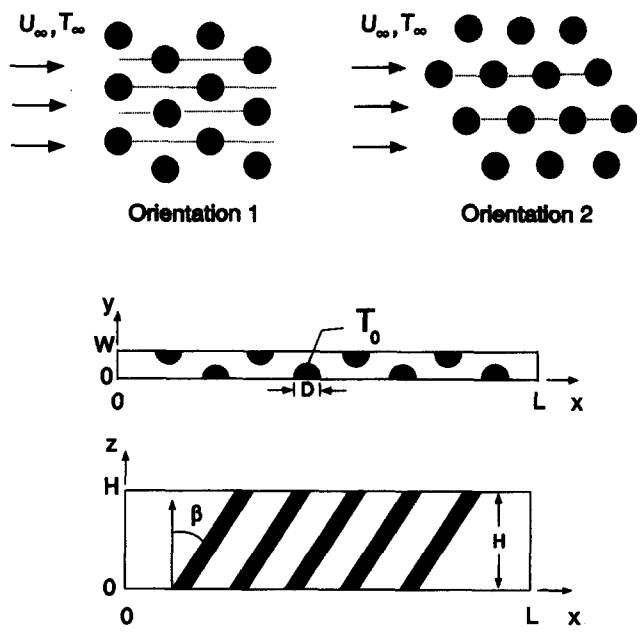

Figure 1 Arrays of parallel cylinders with forced convection heat transfer (*top*), and 3-D computational domain (*bottom*)

not a function of the angle β. In an equilateral triangle array the porosity is $\phi = 1 - 0.907\,(D/S)^2$, where S is the distance between cylinder centers.

In the range $Re_D \leq 30$ the flow is laminar and the wake behind each cylinder is steady and symmetric. This allowed us to view the array as a sandwich of many channels like the one highlighted in the middle of Figure 1 and illustrated by the dashed lines in the top drawings of Figure 1. There was no mixing between the channels. The computational domain contained only one channel.

The equations that account for the conservation of mass, momentum and energy in the fluid regions of the 3-D frame defined in Figure 1 are

$$\frac{\partial u}{\partial x} + \frac{\partial v}{\partial y} + \frac{\partial w}{\partial z} = 0 \tag{1}$$

$$u_j \frac{\partial u_i}{\partial x_j} = -\frac{1}{\rho}\frac{\partial P}{\partial x_i} + \nu \frac{\partial^2 u_i}{\partial x_j^2} \tag{2}$$

$$u\frac{\partial T}{\partial x} + v\frac{\partial T}{\partial y} + w\frac{\partial T}{\partial z} = \alpha\left(\frac{\partial^2 T}{\partial x^2} + \frac{\partial^2 T}{\partial y^2} + \frac{\partial^2 T}{\partial z^2}\right) \tag{3}$$

where (u, v, w) are the velocity components aligned with the (x, y, z) axes. Equation 2 makes use of the tensor notation convention that triple summation is indicated by repeated indices. The boundary conditions on the cylinder surfaces account for no slip, no penetration and uniform temperature,

$$u_i = 0 \quad \text{and} \quad T = T_0 \quad \text{on all cylinder surfaces} \tag{4}$$

Along the top and bottom of the channel and on the side-wall regions contained between cylinders the conditions were zero shear, no penetration and zero heat flux,

$$\frac{\partial u}{\partial z} = 0, \frac{\partial v}{\partial z} = 0, w = 0 \quad \text{and} \quad \frac{\partial T}{\partial z} = 0 \quad \text{at} \quad z = 0, H \tag{5}$$

$$\frac{\partial u}{\partial y} = 0, v = 0, \frac{\partial w}{\partial y} = 0 \quad \text{and} \quad \frac{\partial T}{\partial y} = 0 \quad \text{at} \quad y = 0, W \tag{6}$$

The flow was isothermal and longitudinally uniform at the channel inlet,

$$u = U_\infty, v = 0, w = 0 \quad \text{and} \quad T = T_\infty \quad \text{at} \quad x = 0 \tag{7}$$

The channel outlet conditions were zero stress and zero longitudinal heat flux,

$$-p + 2\mu\frac{\partial u}{\partial x} = 0, \frac{\partial v}{\partial x} = 0, \frac{\partial w}{\partial x} = 0, \frac{\partial T}{\partial x} = 0 \quad \text{at} \quad x = L \tag{8}$$

The equations and boundary conditions were nondimensionalized by using D, U_∞ and $(T_0 - T_\infty)$ as representative scales,

$$(X, Y, Z) = \frac{(x, y, z)}{D}, \qquad (U, V, W) = \frac{(u, v, w)}{U_\infty} \tag{9}$$

$$\theta = \frac{T - T_\infty}{T_0 - T_\infty}, \qquad P = \frac{p}{\rho U_\infty^2} \tag{10}$$

The nondimensional counterparts of Equations 1–8, which are omitted for brevity, contain the nondimensional numbers

$$Re_D = \frac{U_\infty D}{\nu}, \qquad Pr = \frac{\nu}{\alpha}, \qquad (\tilde{H}, \tilde{L}, \tilde{W}) = \frac{(H, L, W)}{D} \tag{11}$$

The system of nondimensional equations was solved using the finite element package FIDAP (1991). When the cylinders are inclined ($\beta \neq 0$) the problem is inherently 3-D, and thus a 3-D solver was required. The computational domain was built up of 8 node brick elements. A Stokes flow solution was used to initialize the solution for the mass and momentum equations when $\beta = 0°$, and then the solution to each prior run was used to initialize the next run, as β was increased. Because the energy equation is only weakly coupled to the mass and momentum equations, it was solved separately for the various Pr values after the velocity field was determined.

Numerical testing indicated that a channel with 40 cylinders in the longitudinal direction allowed for pressure measurements at rows 11, 19 and 27 that were not affected by the entrance or exit regions. We verified that the flow was fully developed by calculating the pressures at three equidistant longitudinal locations (say a, b and c), and checking that the pressure drops

Notation

A	wetted area
$\tilde{A}$	dimensionless wetted area
$\tilde{A}_{flow}$	dimensionless flow cross-sectional area
$B_{h,v,x}$	bias errors
c	constant
c_p	fluid specific heat at constant pressure
D	cylinder diameter
$\tilde{F}$	dimensionless mean velocity, Equation 18
H	height of computational domain
$\tilde{H}$	dimensionless height
K	permeability of porous medium
L	length of computational domain
$\tilde{L}$	dimensionless length
n	constant
Nu	row Nusselt number
p	pressure
P	dimensionless pressure
Pr	Prandtl number
$P_{h,F,v,\rho}$	precision errors
r	exponent
Re_D	Reynolds number
S	distance between cylinder centers
T	temperature
T_0	surface temperature
T_∞	inlet fluid temperature
u_i	velocity components
u, v, w	velocity components
U, V, W	dimensionless velocity components
U_∞	inlet velocity
W	width of computational domain
$\tilde{W}$	dimensionless width
x, y, z	Cartesian coordinates
X, Y, Z	dimensionless Cartesian coordinates

Greek letters

α	fluid thermal diffusivity
β	angle, Figure 1
ΔT_{lm}	log-mean temperature difference
θ	dimensionless temperature
μ	viscosity
ν	kinematic viscosity
ρ	fluid density
ϕ	porosity

matched, $P_a - P_b = P_b - P_c$. In all cases, the discrepancy between the two pressure drops was less than 1 percent.

The effect of doubling the channel height $\bar{H}$ was found to be insignificant (<1 percent change in the pressure gradient) if the $\bar{H} \geq 6$, and a free-slip boundary condition was used at the top and bottom of the channel. The solution proved to be extremely sensitive to changes in channel height when a no-slip condition was imposed on the top and bottom planes of the channel. Convergence testing for the mesh density was performed with $\beta = 45°$. The number of elements was doubled in each direction until such doubling produced a change in the pressure gradient of <3 percent. These tests were performed for each porosity, and for both orientations of the array.

All of the final numerical meshes for determining the pressure gradient required between 20 000 and 35 000 elements. Typically the initial run, which requires a Stokes flow solution for initialization, required 10 to 20 min of CPU time on a Cray Y-MP. The runs that followed generally required about 10 min of CPU time each. The temporary space required for the matrix solver ranged from 500 to several thousands of megabytes. This, in combination with the increased computational cost of doing proper convergence testing, made a supercomputer necessary. The convergence testing for stability in the calculated Nusselt number indicated that twice as many elements were necessary in the x-direction to achieve a 3 percent stability in the Nusselt number than were needed for the same stability in the pressure gradient. To solve for the velocity field on the finer mesh required about 50 min of CPU time on the Cray Y-MP. Three additional minutes were needed to solve the heat-transfer problem for each Prandtl number.

The Nusselt number calculation could not be performed for the entire range defined by $0.6 \leq \phi \leq 0.95$, $0.72 \leq \mathrm{Pr} \leq 100$ and $1 \leq \mathrm{Re_D} \leq 30$. For example, in the case $\phi = 0.6$, $\mathrm{Pr} = 0.72$ and $\mathrm{Re_D} = 10$, the fluid reached thermal equilibrium with the solid almost immediately (i.e., after the first row). In the opposite extreme (e.g., $\phi = 0.95$, $\mathrm{Pr} = 100$, $\mathrm{Re_D} = 10$) the flow was not fully developed thermally at the downstream end of the computational domain, and no fully developed Nu could be reported. As a rule, if Nu varied by more than 5 percent over the 20 inner rows of cylinders, the thermal development was considered incomplete.

Pressure drop results

The results that document the effect of the cylinder angle of inclination on pressure drop are presented in Figures 2a–d. The ordinate shows the pressure gradient in an array with inclined cylinders, as a fraction of the pressure gradient when the same array is perpendicular to the same flow. The first three frames show that when $\mathrm{Re_D} \leq 10$ the relative pressure drop $\Delta P(\beta)/\Delta P(0°)$ is influenced only by the angle β and not by the other parameters ($\mathrm{Re_D}$, ϕ, orientation). The β effect can be significant; for example, in all four frames of Figure 2 the pressure drop decreases to 60 percent of its original value as β increases from 0°–60°.

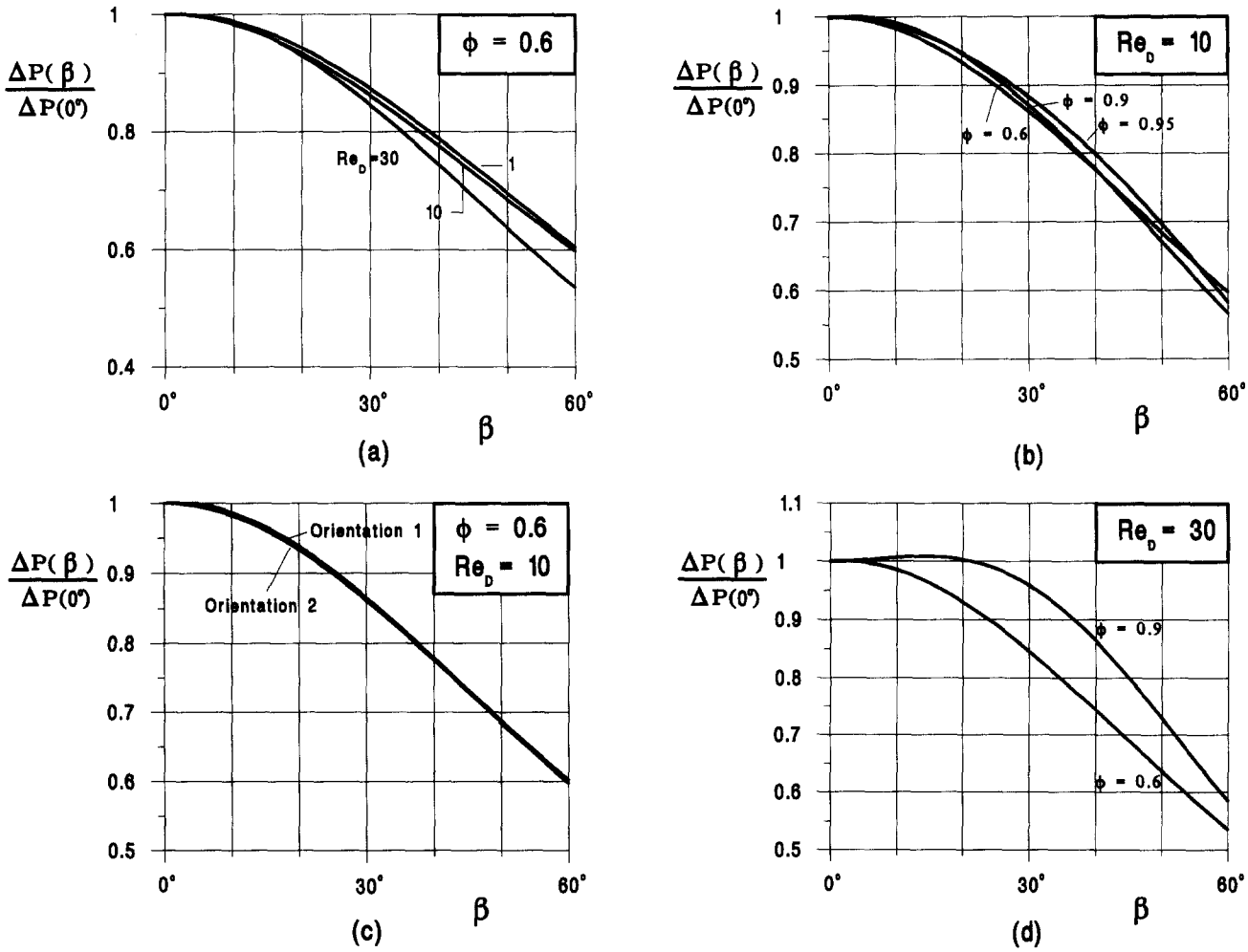

Figure 2 The effect of β, ϕ, $\mathrm{Re_D}$ and array orientation on the longitudinal pressure drop in fully developed flow

Figures 2a and d indicate that at Reynolds numbers larger than 10 the relative pressure drop depends on Re_D and ϕ, in addition to β. The pressure drop is considerably more sensitive to changes in the angle β at low porosities ($\phi = 0.6$) than at high porosities ($\phi = 0.9$). When the porosity is high, the angle of inclination has no visible effect on the pressure drop if $\beta \lesssim 30°$.

These results can be compared with the single relative pressure drop curve reported by Zukauskas (1987), which falls right on top of the curve drawn in Figure 2a for $Re_D = 30$ and $\phi = 0.6$. The present results suggest that the $\Delta P(\beta)/\Delta P(0°)$ curve is not universal (i.e., it is not independent of Re_D and ϕ). This lack of universality is particularly evident in the direction of increasing Re_D, which is the domain of heat exchanger applications. At the same time, the present results show that a universal relative pressure drop curve different than Zukauskas's exists when Re_D is smaller than 10.

We also correlated the pressure drop data for cross-flow ($\beta = 0°$) by modeling the array and the fluid as a saturated porous medium. In the small-Re_D limit the flow is expected to follow the Darcy model,

$$-\frac{\partial p}{\partial x} = \frac{\mu}{K} u \tag{12}$$

The permeability K was determined by fitting the numerical pressure gradient results to Equation 12 and correlating the K values using a formula similar to the Carman-Kozeny relation (Carman 1937),

$$K = \frac{D^2}{125}\left[\frac{\phi^3}{(1-\phi)^2}\right]^r \tag{13}$$

with $r = 0.85$ for orientation 1 and $r = 0.8$ for orientation 2. Equation 13 agrees within 6 percent with the numerical K values deduced from Equation 12 for orientation 1 and $\phi \leq 0.9$. The agreement between Equations 12 and 13 is within 35 percent for all the runs made for orientation 2: the average error for all the runs in both orientations was 10 percent. The agreement for the runs in orientation 2 is illustrated in Figure 3, where the numbers listed after each point represent Re_D and ϕ. The use of $K^{1/2}$ as length scale in the dimensionless groups on the ordinate and abscissa of Figure 3 is standard in the field of convection in porous media (Cheng 1978; Nield and Bejan 1992). Equation 12 is not shown in the figure: it would be represented by a line of slope -1 passing through the point (1, 1), that is, a line that would pass right through the shown data.

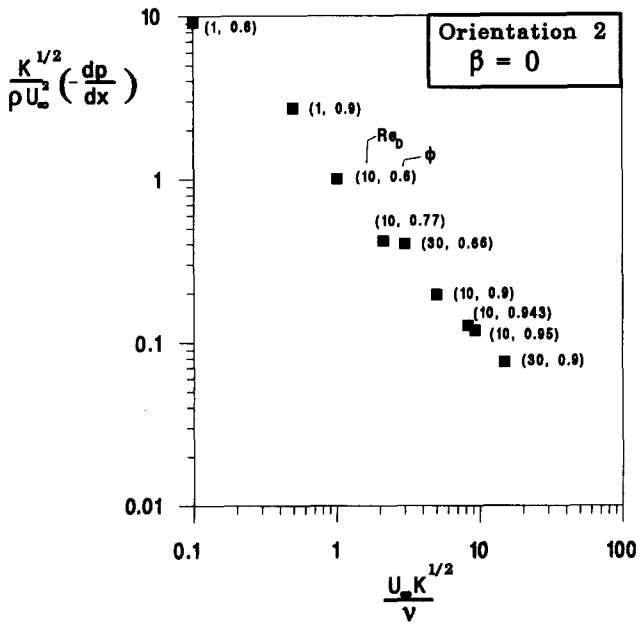

Figure 3 Porous-medium correlation of the pressure drop results for cross-flow

Heat-transfer results for cylinders in cross-flow

The results of the heat transfer part of the problem defined in the mathematical formulation section are summarized as an average Nusselt number

$$\mathrm{Nu} = \frac{hD}{k} \tag{14}$$

The rate of heat transfer between the fluid and the wetted area A in any control volume of the computational domain is

$$q = hA\Delta T_{\mathrm{lm}} = \dot{m} c_p (T_{\mathrm{out}} - T_{\mathrm{in}}) \tag{15}$$

where $\dot{m}$ is the mass flow rate through the domain (Figure 1, *bottom*). The relation between Nu and the nondimensional formulation presented in the mathematical formulation section is

$$\mathrm{Nu} = \frac{\tilde{F}\mathrm{Re}_D \mathrm{Pr}(\theta_{\mathrm{out}} - \theta_{\mathrm{in}})}{\tilde{A}\theta_{\mathrm{lm}}} \tag{16}$$

where $\tilde{A} = A/D^2$ and

$$\theta_{\mathrm{lm}} = \frac{\theta_{\mathrm{out}} - \theta_{\mathrm{in}}}{\ln[(1-\theta_{\mathrm{in}})/(1-\theta_{\mathrm{out}})]} \tag{17}$$

$$\tilde{F} = \int_{\tilde{A}_{\mathrm{flow}}} U d\tilde{A}_{\mathrm{flow}} \tag{18}$$

Experimental studies usually report Nu averaged over the entire array, because that value is experimentally accessible. We calculated the "local" Nusselt number associated with (averaged over) a certain row of cylinders to monitor the thermal development of the flow, from one row to the next.

The results obtained for $\beta = 0°$ show that in general the row Nusselt number Nu in the first few rows is larger than in later rows. This trend is illustrated in Figure 4. We found that the Nu value for the first row was very sensitive to grid refinement.

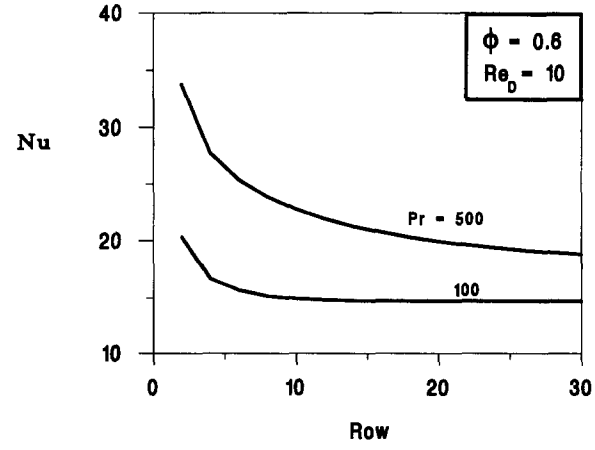

Figure 4 The local (row) Nusselt number as a function of Pr and longitudinal position

Table 1 Constants for the fully developed Nusselt number correlation (Equation 20)

ϕ	c	n
0.6	5.64	0.14
0.9	2.34	0.18
0.95	2.0	0.18

After a few rows Nu approached a constant, which was less sensitive to grid refinement. Our convergence tests were based on the stability of the constant Nu value found between rows 7–31.

The only correlation for low Reynolds number heat transfer for staggered tube banks in cross-flow appears to be a formula by Zukauskas (1987a).

$$\mathrm{Nu} = 1.04\,\mathrm{Re}_{D,f}^{0.4}\mathrm{Pr}^{0.36}\left(\frac{\mathrm{Pr}_f}{\mathrm{Pr}_w}\right)^{0.25} \tag{19}$$

where Nu is the value for "inner rows," and $\mathrm{Re}_{D,f}$ is based on the velocity averaged over the minimum cross section. Equation 19 was recommended for the range $1.6 < \mathrm{Re}_{D,f} < 40$. The subscripts $_f$ and $_w$ indicate that the properties must be evaluated at the flow mean temperature and, respectively, the cylinder surface temperature.

Our results for fully developed cross-flow in the range $1 \le \mathrm{Re}_D \le 30$ and $0.72 \le \mathrm{Pr} \le 100$ are correlated by the power law

$$\mathrm{Nu} = c(\mathrm{Re}_D\,\mathrm{Pr})^n \tag{20}$$

for which the constants c and n are reported in Table 1. The agreement between the numerical Nu values and the values obtained based on Equation 20 is within 4 percent.

The most important difference between the correlations (Equations 19 and 20) is the smaller exponent n (i.e., weaker Re_D and Pr effect) present in Equation 20. To understand these differences we examined the experimental and numerical work on which Equation 19 is based (Bergelin et al. 1949, 1950; Omohundro et al. 1949). For example, Equation 20 underestimates by a factor of 2 the Nusselt number found experimentally by Bergelin et al. (1950) for $\mathrm{Pr} \cong 500$. The numerical work of Chang et al. (1989), which was performed for $\mathrm{Pr} = 0.7$, agrees with the Bergelin et al. experiments when a $\mathrm{Pr}^{0.33}$ correction factor is applied to the Nusselt number. The agreement between Bergelin et al. and Chang et al. is due to the shortness of the arrays studied (10 rows for Bergelin et al. and 5 rows for Chang et al.), and explains why Equations 19 and 20 are different.

Figure 4 illustrates the effect of the Prandtl number on the local Nusselt number over the first 30 rows. When we examine our numerical results for the first 10 cylinder rows we find that the Nusselt number averaged over 10 rows scales as $\mathrm{Pr}^{0.3}$ and that our numerical simulation agrees with the findings of Bergelin et al. to within 10 percent. Nonetheless at later rows where the flow is fully developed, our correlation (Equation 20) applies. For flow systems in which the flow becomes fully developed early in the array, it is clear that Zukauskas's formula (Equation 19) would result in significant error (although it is correct for short arrays in which entrance effects dominate).

The same explanation (fully developed flow *vs.* entrance flow) holds for the different exponents on the Reynolds number in Equations 19 and 20. That the Nusselt number in the fully developed region is proportional to Re_D^n where n is significantly smaller than in Zukauskas's correlation (Equation 19) is further supported by the experiments of Minakami et al. (1993). These authors tested an array of in-line square pin fins with 10 to 20 rows in the longitudinal direction, and found that $\mathrm{Nu} \sim \mathrm{Re}_D^n$, where n is between 0.2 and 0.25 in the laminar regime and for $\mathrm{Pr} = 7$ (water). Comparison of our findings with the results of Minakami et al. (1993) is reasonable because the shape of the pins (square or cylindrical) should have only a small effect in the low Re_D regime. Furthermore, Zukauskas (1987a) indicates that Nu values for staggered and in-line arrays have the same Re_D dependence for $\mathrm{Re}_D > 40$.

Heat transfer results for inclined cylinders

Zukauskas (1972) proposed the single curve of Figure 5 (*top*) as a heat-transfer method of accounting for the effect of the angle of inclination β between the cylinder axis and the direction perpendicular to the flow. He did not indicate the Re_D range and array dimensions for which this curve is valid. Our results for fully developed flow, $1 \le \mathrm{Re}_D \le 30$, $0.72 \le \mathrm{Pr} \le 100$, and orientation 1 indicate that the angle effect on Nu is considerably smaller than indicated by Zukauskas.

Groehn (1981) proposed the principle of independence as a method of accounting for the effect of β on the Nusselt number. In this method the relevant velocity scale is that normal to the cylinder; hence, the Reynolds number that should be used in Equation 20 is $\mathrm{Re}_D \cos\beta$. If the principle of independence is valid then the ratio $\mathrm{Nu}(\beta)/\mathrm{Nu}(0°)$ should be a function of ϕ and

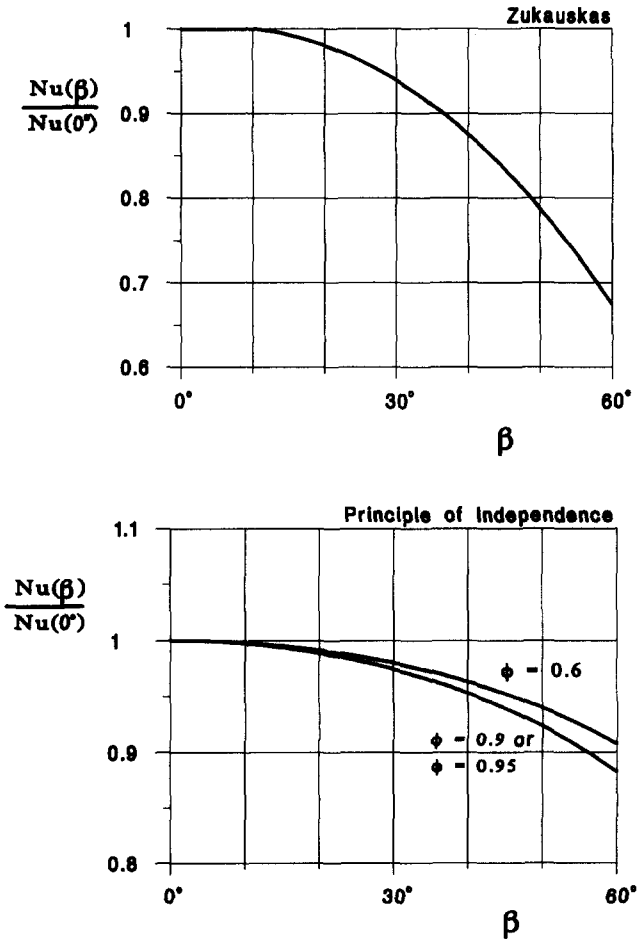

Figure 5 Zukauskas's (1972) curve for the effect of the angle β on the Nusselt number (*top*); the principle of independence in combination with Equation 20 (*bottom*)

β only. Figure 5 (*bottom*) illustrates the curves predicted by the principle of independence in combination with Equation 20.

Figures 6a–c show how the ratio $Nu(\beta)/Nu(0°)$ responds to changes in β, ϕ and Pr when Re_D is fixed. An interesting feature is the evolution of the Pr = 7 curve (e.g., water) as the porosity increases from 0.6–0.95. The $Nu(\beta)/Nu(0°)$ curve moves upward as ϕ increases, and this means that the angle effect is weaker in a sparse array than in a dense array. In particular, when $\phi = 0.95$ and $0° < \beta \lesssim 45°$ the Nusselt number for inclined cylinders is greater than for the same array in cross-flow. This feature is almost the same as in the experimental results of Willins and Griskey (1975), who measured the mass transfer from a single cylinder inclined relative to a uniform flow. In the Willins and Griskey experiment the group $Re_D Sc$ was of the order of 10^4 (note that $Re_D Sc$ is the mass-transfer equivalent of the Peclet number in forced convection heat transfer). In Figure 6c, the Pr = 7 curve corresponds to $Pe_D = 70$, which is the highest Peclet number illustrated in that frame. Moreno and Sparrow (1987) found an increase in Nu at small angles β in flow through tube banks at $Re_D \sim 10^4$ if the cylinders were in line, but not if they were staggered. As our array becomes more sparse, it more closely approximates the in-line configuration. In conclusion, Figure 6c, Willins and Griskey's and Moreno and Sparrow's results suggest that the increase in $Nu(\beta)$ and $Nu(0°)$ in a small β range is a high Peclet number effect visible in in-line arrays, sparse staggered arrays or isolated cylinders.

Figure 7 shows how the Nusselt number behaves at constant Pr and constant Re_D. The curves show that the porosity has a relatively weak effect and that the ratio $Nu(\beta)/Nu(0°)$ is mainly a function of β. Again, the exception is the $\phi = 0.95$ curve in Figure 7b, which shows that the porosity plays a role when the array is sufficiently sparse.

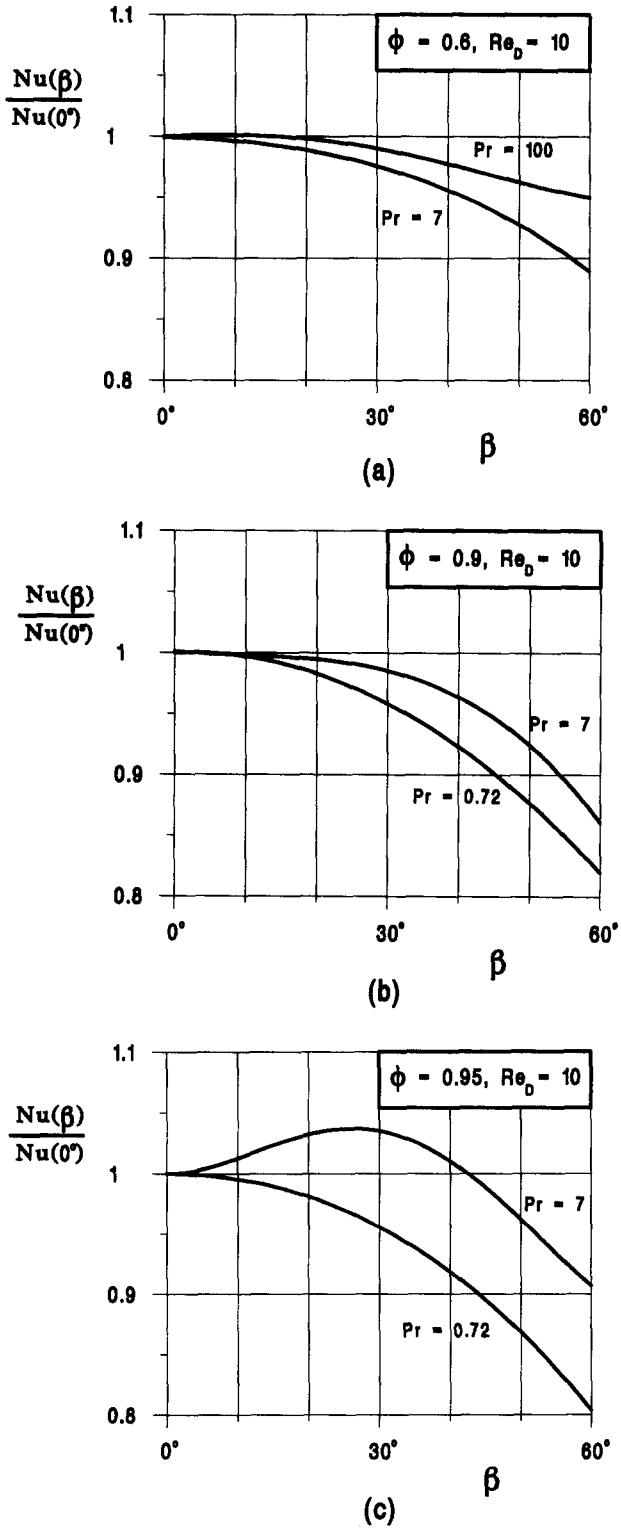

Figure 6 The effect of angle of inclination, Prandtl number and porosity on the Nusselt number ($Re_D = 10$)

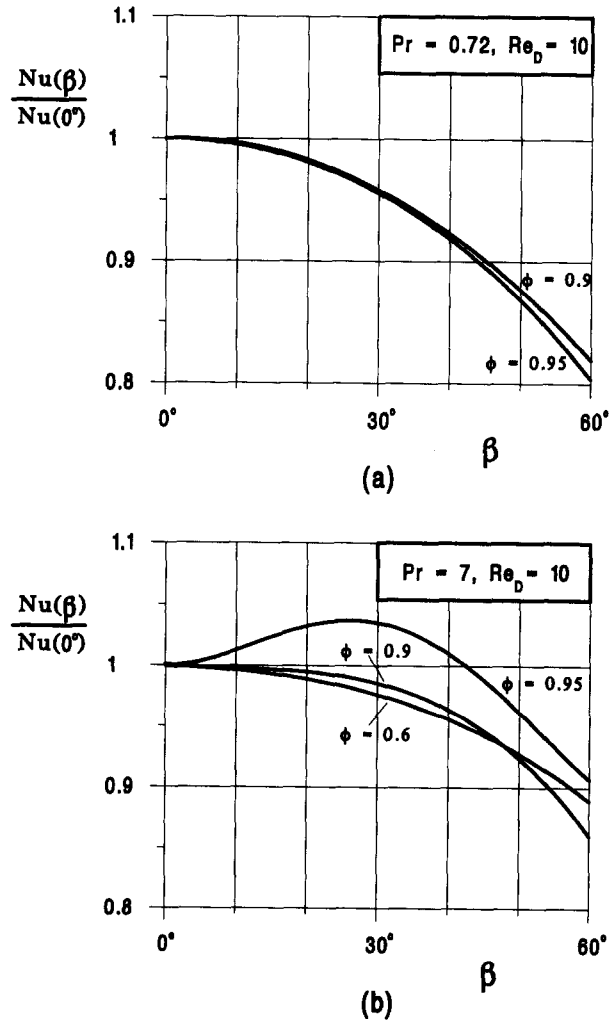

Figure 7 The effect of angle of inclination and porosity when Re_D and Pr are fixed

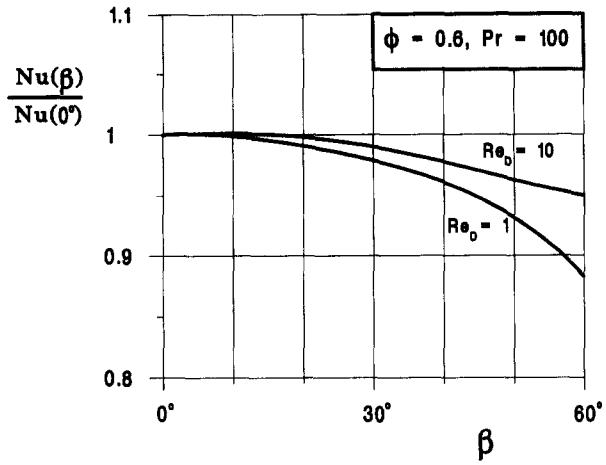

Figure 8 The effect of the Reynolds number on the Nusselt number of an inclined array

Figure 8 shows that the Re_D effect is such that $Nu(\beta)/Nu(0°)$ increases when Re_D increases. This is interesting because it means that the $Nu(\beta)/Nu(0°)$ curve becomes less and less like Zukauskas's curve (Figure 5) as Re_D increases. This trend is the opposite of what we found in the results for the pressure drop, where the $\Delta P(\beta)/\Delta P(0°)$ curve approached Zukauskas's curve as Re_D increased (Figure 2a).

Finally, in Figures 9a and b we show that when the Peclet number ($Pe_D = Re_D Pr$) is held constant (of order 100), the ratio $Nu(\beta)/Nu(0°)$ is essentially a function of β only. Plotted are two curves ($Pe_D = 70$ and 100) for $\phi = 0.6$ and $\phi = 0.9$, and a single point ($Re_D = 30$, $Pr = 3.3$) for $\phi = 0.6$. Comparing this finding with the relative pressure curves of Figure 2 leads to the conclusion that when the relative pressure curve is independent of Re_D (namely, when $Re_D \leq 10$), the ratio $Nu(\beta)/Nu(0°)$ is a function of β and Pe_D, and not of Re_D and Pr separately.

The dependence of $Nu(\beta)/Nu(0°)$ on Pr and Re_D indicates that the principle of independence does not hold in a strict sense. It does, however, provide a good order-of-magnitude estimate for the effect of β. That the principle of independence does not hold exactly in the low Re_D regime is reasonable, because this principle is based on the assumption that the flow away from the cylinder surface is inviscid.

The most important aspect of the heat-transfer results presented in this section is that at low Reynolds numbers the effect of cylinder inclination is relatively small, regardless of the Peclet number. For example, if the β effect is ignored in the estimation of Nu in the β range 0°–60°, the error in Nu is less than 20 percent.

Experiments for pressure drop

We verified the accuracy of our numerical results by measuring in the laboratory the pressure drop across a long bundle of cylinders with several inclinations ($\beta = 0°, 45°, 60°$) and at low Reynolds numbers ($8 \lesssim Re_D \lesssim 50$). We chose to test the pressure drop calculations because they represent the most critical part of the results described until now, because the effect of cylinder inclination is much greater on the pressure drop than on the heat-transfer coefficient. We needed to verify that our computational domain captured correctly the 3-D flow effects present in an array with many yawed and long cylinders. Earlier experimental studies of low-Re_D flows through cylinders in cross-flow (Bergelin et al. 1949, 1950; Omohundro, 1949) were limited by the fact that the arrays were too short, and the flows were not fully developed. Furthermore, we could not find any experimental reports on low-Re_D flows through inclined cylinder arrays.

Apparatus

The main features of the experimental apparatus are shown in Figure 10. We constructed an array with 12 cylinders across and 115 cylinders in the flow direction, with the cylinders arranged in the configuration indicated as orientation 1 in Figure 1. The length of the array was 60 cm. The cylinders were made of 0.07-inch (1.8-mm) rubber O-ring stock. They were 7.4 cm long and spaced in equilateral triangles with side length of 6 mm. When the cylinders were oriented across the flow ($\beta = 0°$) the porosity of the array was $\phi = 0.92$. The channel height to cylinder diameter ratio was 420:1. To change the fiber angle, the wall of the lower channel was shifted longitudinally and upward, such that the total fiber length remained the same (7.4 cm), but the distance between the top and bottom of the channel changed, and the fiber angle changed. When $\beta = 60°$ the channel height to cylinder ratio was 210:1 and the porosity was $\phi = 0.84$.

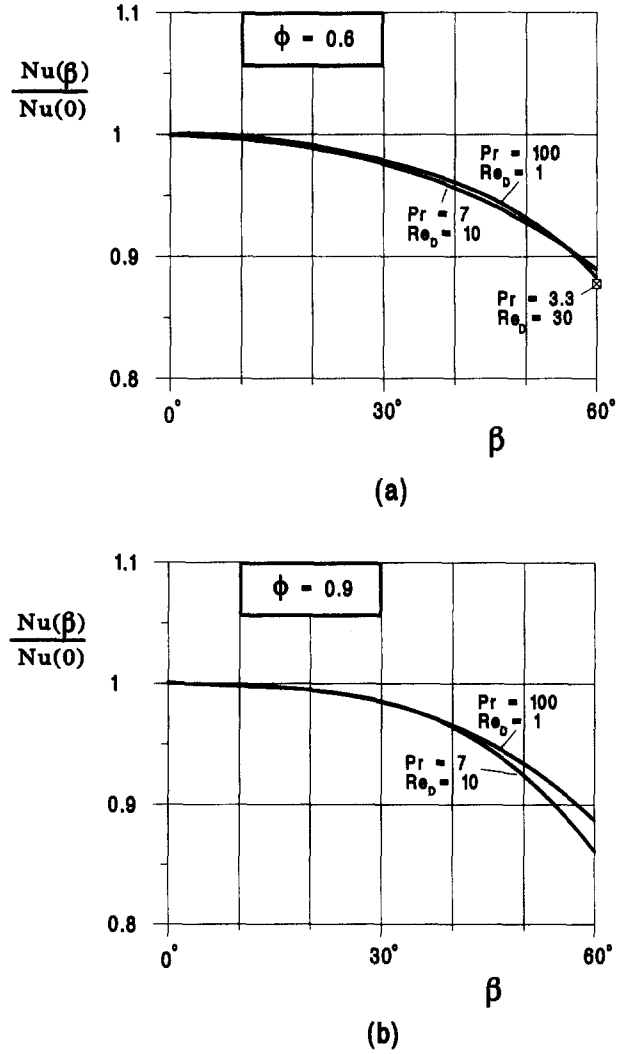

Figure 9 The angle effect on the Nusselt number when the array is dense and the Peclet number is fixed

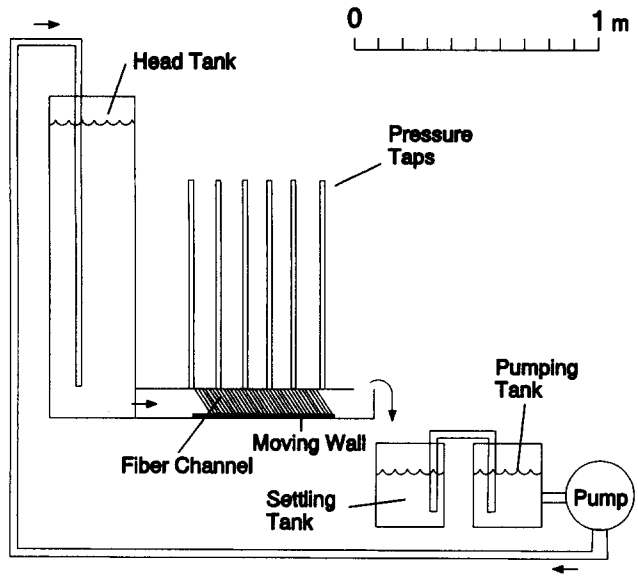

Figure 10 The main components of the experimental apparatus

The fiber channel was connected to a 2-m tall tank into which fluid could be pumped, thereby developing a pressure head to drive flow through the array. Six manometers were spaced along the channel so that pressure measurements could be made in the region of fully developed flow. The fluid drained out of an opening at the end of the fiber channel into a settling tank, from which it was siphoned into the pumping tank and repumped into the head tank.

The pump operated at constant flow rate during each run, so that the height of the fluid column in the head tank adjusted itself until the flow rate through the fiber channel matched the flow rate into the head tank. We measured the flow rate by timing the filling of a container placed under the exit from the fiber channel. The fluid was a solution of corn syrup and water (ratio 1:3 by volume) with a kinematic viscosity between $7–8 \times 10^{-6}$ m^2/s. The viscosity depended on the temperature and the concentration of corn syrup, and varied from day to day but was stable during a series of consecutive runs. It was measured after each run with a Cannon-Fenske–type viscometer.

The pump was a variable speed Simer shallow well pump. The manometers were glass tubes with 4 mm inside diameter and 1 m height. The head tank and the walls of the fiber channel were made of Lexan. The fibers (total number $\approx$ 1380) were tied on the back side of orifices drilled in the top and bottom walls of the fiber channel, and sealed with RTV silicone sealant. The fibers were pulled tight to prevent bending during operation. No bending or vibration of the fibers was observed; however, only the outermost fibers could be seen because of the density of the fibers.

Procedure

The pump was set at a certain flow rate. After the pump had run for a few minutes, to let the bubbles flow out and to allow the head tank to reach its equilibrium height, the liquid levels in the manometers were read and recorded. Then the fill time for a 1-gallon container collecting fluid at the fiber channel exit was measured 5 times. Finally, the manometer levels were read again to make sure that steady state had been achieved.

Four of the manometers were positioned in the region of fully developed flow. After a few runs it became clear that it was going to be unusual to produce a run in which all four manometers were bubble-free at the time of measurement. To maintain consistency between runs, the reading of one manometer was discarded from every run. Pressure was determined by the relationship $P = \rho g h$, where ρ is the measured fluid density, g is gravitational acceleration, and h is the height of the column measured in the manometer. The fluid density was measured by weighing a 10-ml fluid sample. A 95 percent confidence interval was calculated based on the three pressure measurements. Only in the case of one run was the precision error found to be greater than 5 percent, and the run was discarded. All other runs for which all of the necessary measurements could be made were included in the reported results.

The longest and shortest measured times for flow rate were discarded, and the remaining 3 times were averaged to find the flow rate and to calculate the precision error. The fluid velocity derived from this measurement was the average channel velocity, which is equivalent to the inlet velocity U_∞ used in the numerical simulations.

Error analysis

All errors were calculated using 2 standard deviations as the 95 percent confidence interval. There were four sources of precision error in this experiment (random errors and unsteadiness): the height measurements in the manometers P_h, the kinematic viscosity measurements P_ν, the density measurements P_ρ, and the flow-rate measurements P_F. The precision errors P_h and P_F changed from run to run. The precision error for density ($P_\rho/\rho \sim 0.07$ percent) was negligible compared to other errors and did not vary from run to run. Repeated tests for kinematic viscosity in which fluid samples were taken from different tanks in the system indicated that $P_\nu/\nu = 2.2$ percent.

The bias, or the fixed errors for height and distance measurements, were calculated assuming that our ruler was accurate to within ± 0.5 mm. Because the heights being measured changed depending on flow rate, B_h/h varied with each run, between 0.5–4 percent. The fixed error for the gallon container was estimated by repeated calibration against highly accurate volumetric measuring containers and was found to be 1 percent. Because of the extremely accurate containers, scales and viscometer calibration, the bias errors for those measurements were negligible compared with the height and gallon volume errors. The non-negligible bias and precision errors that did not vary from run to run are listed in Table 2.

The 95 percent confidence was determined by combining all bias and precision errors using the root-sum-square method, and is indicated graphically for each point plotted in Figures 11 and 12. The data scatter falls within the estimated errors.

Results

Figure 11 shows the experimental points for $\beta = 0°$, and the corresponding numerical results (the solid line). Note again that U is the volume averaged velocity, equivalent to U_∞ of the numerical simulations. The Reynolds numbers covered by the data vary between 10–50. Our numerical solution becomes less accurate for $Re_D > 30$. A possible explanation for this is that the experimental system enters the transition to the turbulent

Table 2 Non-negligible bias and precision errors

P_ν/ν (percent)	B_x/x (percent)	B_v/V (percent)	P_ρ/ρ (percent)
2.19	0.5	1	0.07

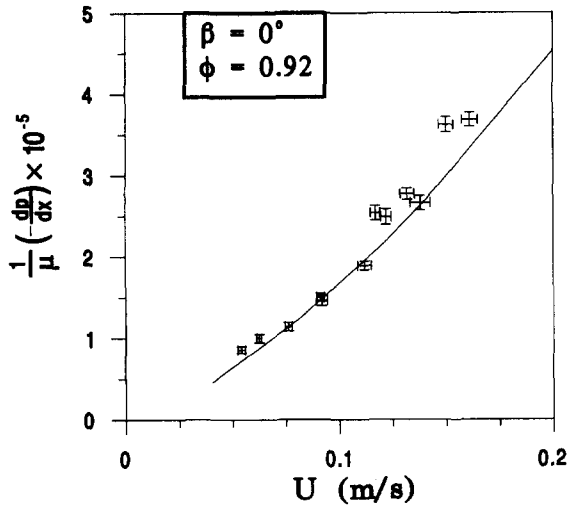

Figure 11 Comparison between the experimental and numerical results for cylinders in cross-flow

regime for higher Re_D. This behavior is suppressed in our numerical simulation by the assumption of impermeable side walls for the computational domain. These boundary conditions do not allow the flow to meander. The numerical and experimental results show very clearly that for low Re_D the flow is approximately Darcy flow and that the numerical simulation predicts the permeability of the array extremely well.

Figure 12a shows the experimental results for $\beta = 60°$ compared with the numerical solution that corresponds to the experimental geometry. The number of elements, the boundary conditions and general configuration used in the simulation were the same as those used in our earlier numerical work (see earlier discussion). An adjustment was made to account for the specific geometry of the experimental system. Unlike our earlier numerical work, in the experiment the porosity is a function of the angle β, and the fibers are no longer arranged in equilateral triangles when $\beta \neq 0$. The two curves in Figure 12a show the numerical solution for the experimental geometry at $\beta = 0°$ and 60°. The agreement between the experimental and numerical results is excellent.

The results illustrated in Figure 12a cover the Re_D range 10–50. In the $\beta = 60°$ array, where the porosity is lower than when $\beta = 0°$, the Darcy regime covers a wider Re_D range, and our numerical results agree with the measurements reasonably well over the entire Re_D domain.

Figure 12b shows the experimental data for $\beta = 60°$ next to the prediction based on the porous medium flow model (Equation 12). In this model we combined the permeability from Equation 13 with the angle effect documented in Figures 2b and d. The agreement between the proposed model and the experimental data is excellent. We cannot make a similar comparison for $\beta = 0°$ because it falls outside the Darcy regime (the array orientation is 1, and the porosity is greater than 0.9).

Figure 13 shows the experimental and numerical results for $\beta = 45°$. There are no error bars on these data points because in this configuration we could not verify the precision error: the angle was such that the entrance and end region effects penetrated to two of the central pressure taps that were supposed to be in the fully developed flow region. Thus only two pressure taps were in the fully developed region, and only one pressure gradient measurement was possible. The pumping mechanism was not precise enough to duplicate exactly the flow conditions for two successive runs, and, therefore, to repeat runs while holding the velocity constant was not

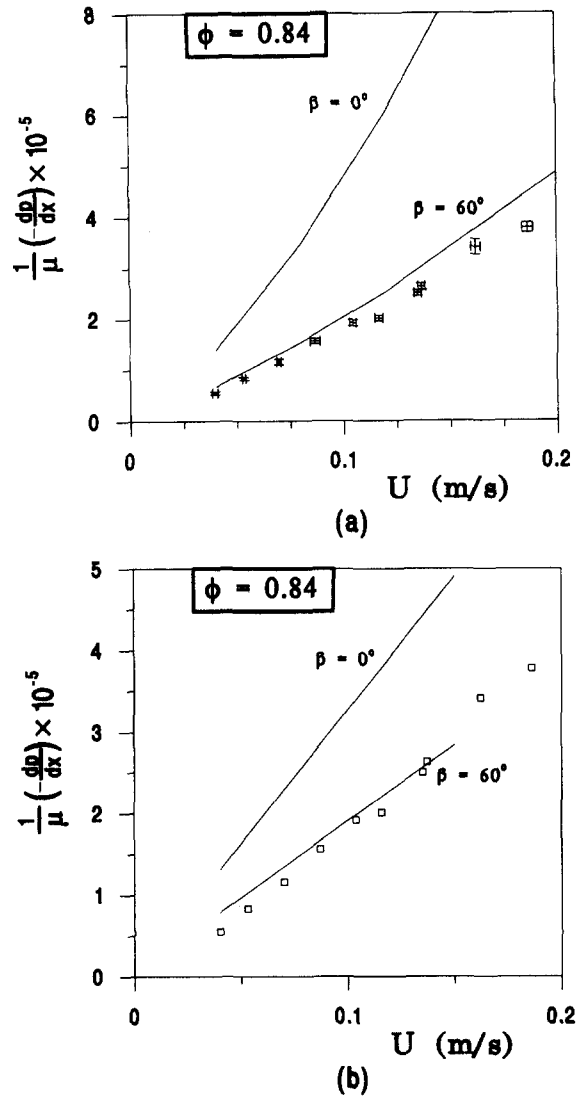

Figure 12 Cylinders inclined at 60° relative to the cross-flow position: (a) comparison between experimental and numerical results, and (b) comparison between the porous medium model (Equation 12) and the experimental results

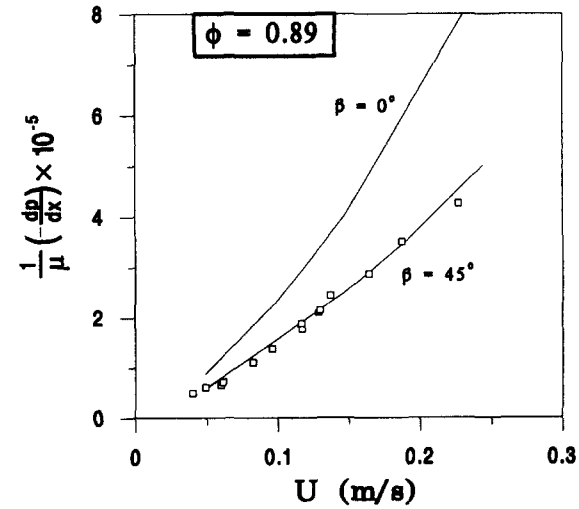

Figure 13 Comparison between the experimental and numerical results for the array inclined at 45°

possible. Instead the experiment was run repeatedly at approximately the same flow rate. If repeated pressure gradient measurements indicated that the first run was not corrupted by an unseen bubble or other anomaly (i.e., if two runs of roughly the same flow rate showed roughly the same pressure drop, the measurement produced by the first run was plotted). The consistency of the data plotted in Figure 13 is strong evidence that the measurements are sufficiently accurate, and they agree very well with the numerical prediction.

Conclusion

In this article we documented the pressure drop and heat transfer characteristics of flows through bundles of parallel cylinders when

1. The Reynolds number is low.
2. The flow is hydrodynamically and thermally fully developed.
3. The cylinders may be inclined relative to the flow direction.

These three aspects had not been documented before, yet they are very important in applications with length scales smaller than the scales of conventional heat exchanger technology.

The results of this study demonstrate that the parametric domain represented by aspects 1–3 requires special attention and that significant errors may occur if the available large-scale (heat exchanger-type) information is extrapolated to smaller scales. For this reason, a useful direction for future research would be to generate more data for pressure drop and heat transfer in the domain 1–3. Another direction would be to widen the Reynolds number range to Re_D values as high as 100, that is, to cover the transitional regime where the flow behind each cylinder meanders (e.g., Minakami et al. 1993) and the symmetry assumed in Figure 1 (*top*) breaks down.

Acknowledgments

The present study was supported by the Air Force Office of Scientific Research. The experimental apparatus was constructed by Michael Gunter. The computational work was made possible by a grant from the North Carolina Supercomputing Center. The computational assistance received from Professor Laurens Howle is gratefully acknowledged.

References

Bergelin, O. P., Davis, E. S. and Hull, H. L. 1949. A study of three tube arrangements in unbaffled tubular heat exchangers, *Trans. ASME*, **71**, 369–374

Bergelin, O. P., Brown, G. A., Hull, H. L. and Sullivan F. W. 1950. Heat transfer and fluid friction during viscous flow across banks of tubes: III. *Trans. ASME*, **72**, 881–888

Carman, P. C. 1937. Fluid flow through granular beds. *Trans. Inst. Chem. Eng.*, **15**, 150–166

Chang, Y., Beris, A. N. and Michaelides, E. E. 1989. A numerical study of heat and momentum transfer for tube bundles in crossflow. *Int. J. Num. Meth. Fluids*, **9**, 1381–1394

Cheng, P. 1978. Heat transfer in geothermal systems. *Adv. Heat Transfer*, **14**, 1–105

FIDAP Theoretical Manual, 1991. Fluid Dynamics International, Evanston, IL, V.6.02

Groehn, H. G., 1981. Thermal hydraulic investigation of yawed tube bundle heat exchangers. *Heat Exchangers Thermal-Hydraulic Fundamentals and Design*, S. Kakac, A. E. Bergles and F. Mayinger, (eds.). Hemisphere, Washington, DC, 97–109

Kays, W. M. and London, A. L. 1984. *Compact Heat Exchangers*, 3rd ed., McGraw Hill, New York

Minakami, K., Mochizuki, S., Murata, A., Yagi, Y. and Iwasaki, H. 1993. Heat transfer characteristics of the pin-fin heat sink (mechanism and effect of turbulence in the pin array). *The 6th Int. Symposium on Transport Phenomena in Thermal Engineering*, Seoul, Korea, 67–72

Moreno, A. A. Y. and Sparrow, E. M. 1987. Heat transfer, pressure drop, and fluid flow patterns in yawed tube banks. *Int. J. Heat Mass Transfer*, **30**, 1979–1995

Nield, D. A. and Bejan, A. 1992. *Convection in Porous Media*. Springer-Verlag, New York

Omohundro, G. A., Bergelin, O. P. and Colburn, A. P. 1949. Heat transfer and fluid friction during viscous flow across banks of tubes. *Trans. ASME*, **71**, 27–34

Willins, R. E. and Griskey, R. G. 1975. Mass transfer from cylinders at various orientations to flowing gas streams. *Canadian J. Chemical Eng.*, **53**, 500–504

Zukauskas, A. 1972. Heat transfer from tubes in cross flow. *Adv. Heat Transfer*, **8**, 93–160

Zukauskas, A., 1987a. Heat transfer from tubes in crossflow. *Adv. Heat Transfer*, **18**, 87–159

Zukauskas, A. 1987b. Convective heat transfer in cross flow. *Handbook of Single-Phase Convective Heat Transfer*, S. Kakac, R. K. Shah and W. Aung, (eds.). Wiley, New York, chap. 6